Automatic Parameter Optimization of the Local Model Fitting Method for Single-shot Surface Profiling

Syogo Mori
Tokyo Institute of Technology
2-12-1 O-okayama, Meguro-ku, Tokyo, 152-8552, Japan.
mori@sg.cs.titech.ac.jp

Masashi Sugiyama
Tokyo Institute of Technology
2-12-1 O-okayama, Meguro-ku, Tokyo 152-8552, Japan.
sugi@cs.titech.ac.jp, http://sugiyama-www.cs.titech.ac.jp/~sugi

Hidemitsu Ogawa
Toray Engineering Co., Ltd.
1-1-45 Oe, Otsu, Shiga, 520-2141, Japan.
hidemitsu-ogawa@kuramae.ne.jp

Katsuichi Kitagawa
Toray Engineering Co., Ltd.
1-1-45 Oe, Otsu, Shiga, 520-2141, Japan.
katsuichi_kitagawa@toray-eng.co.jp

Kei Irie
Toray Engineering Co., Ltd.
1-1-45 Oe, Otsu, Shiga, 520-2141, Japan.
kei_irie@toray-eng.co.jp

Abstract

The *Local model fitting* (LMF) method is a single-shot surface profiling algorithm. Its measurement principle is based on the assumption that the target surface to be profiled is *locally* flat, which enables us to utilize the information brought by nearby pixels in the single interference image for robust local model fitting. Given that the shape and size of the local area is appropriately determined, the LMF method was demonstrated to provide very accurate measurement results. However, the appropriate choice of the local area often requires prior knowledge on the target surface profile or manual parameter tuning. To cope with this problem, we propose a method for automatically determining the shape and size of local regions only from the single interference image. The effectiveness of the proposed method is demonstrated through experiments.

1 Introduction

Optical surface profiling can be used for the inspection of various industrial products such as semi-conductors and flat-display panels. The *phase-shift method* [1], which uses multiple interference images taken by changing the relative distance between the target object and the reference mirror, is a classic but useful surface profiling algorithm. Although the phase-shift method was shown to be very accurate, its high accuracy is vulnerable to vibration, and its measurement speed is rather slow due to the need for taking several interference images.

In order to overcome these weaknesses, 'single-shot' surface profiling methods have been developed. A key idea of single-shot methods is to slightly tilt the reference mirror so that the interference patterns can be observed *spatially*. Single-shot methods are fast and robust against vibration, and furthermore the measurement system can be highly simplified since mechanical devices such as piezo actuators are not necessary. For these reasons, various fundamental single-shot methods have been developed so far, e.g., the *Fourier transform method* [2], the *spatial-phase synchronization method* [3], the *windowed Fourier transform method* [4], the *spatial phase-shift method* [5, 6], and the *local model fitting (LMF) method* [7]. Furthermore, more elaborate single-shot algorithms are studied recently [8, 9, 10, 11].

Among these single-shot methods, the LMF method was shown to be particularly useful. Its measurement principle relies on the assumption that the target surface to be profiled is *locally* flat. This assumption enables us to utilize the information brought by nearby pixels in the single interference image for robust local model fitting. The locality of LMF allows us to measure objects with sharp steps and/or covered with heterogeneous materials, which is an advantage over the Fourier transform method and the spatial-phase synchronization method. The windowed Fourier transform method also processes the fringe image locally, but it requires an assumption that the target surface to be profiled is sufficiently smooth. The spatial phase-shift method is accurate, but it requires the reference mirror to be exactly tilted to a specified angle, which is hard to achieve in practice. On the other hand, the tilting angle of the reference mirror can be arbitrary in LMF.

However, the accuracy of the LMF method depends on the choice of local regions, which needs to be manually tuned appropriately in practice. The purpose of this paper is to give a method for automatically determining such tuning parameters only from the single interference image. Our key idea is that a pixel is held out from the estimation of the surface profile, and it is used for validating the accuracy of the estimation. Based on this hold-out validation, tuning parameters such as the size of local regions are determined so that the validation error averaged over the entire image is minimized.

The rest of this paper is structured as follows. In Section 2, we briefly review the LMF method and illustrate its sensitivity to the choice of a tuning parameter through computer simulation. Then we describe our proposed method for automatically determining the tuning parameter value. In Section 3, we extend our automatic parameter optimization method to a flexible variant of LMF called the *iteratively-reweighted LMF* (IRLMF) method [12]. Its practical usefulness is demonstrated through computer simulation and actual experiments. Finally, we conclude this paper in Section 4.

2 Automatic Parameter Determination for Local Model Fitting

In this section, we describe a method for automatically determining tuning parameters included in the LMF method.

2.1 The Local Model Fitting Method

First, let us briefly review the measurement principle of the LMF method [7]. We tilt the reference mirror in an arbitrary angle. Then an interference pattern is modeled as

$$g(x,y) := a(x,y) + b(x,y)\cos\left(\phi(x,y) + 2\pi f_{\mathrm{x}} x + 2\pi f_{\mathrm{y}} y\right), \tag{1}$$

where $a(x,y)$ and $b(x,y)$ are the bias and the amplitude, $\phi(x,y)$ contains information on the surface profile, and f_{x} and f_{y} are the spatial carrier-frequencies along the x- and y-axes, respectively.

In the LMF method, we assume that $a(x,y)$, $b(x,y)$, and $\phi(x,y)$ are constant in the vicinity of a target point (x_t, y_t) on the surface. Let $\mathcal{T}_t$ be the set of indices of pixels in the vicinity of (x_t, y_t). Note that $\mathcal{T}_t$ includes the target point (x_t, y_t) itself. Then the local model around (x_t, y_t) is given and expressed as

$$\begin{aligned}\bar{g}_t(x,y) &:= a_t + b_t\cos(\phi_t + 2\pi f_{\mathrm{x}} x + 2\pi f_{\mathrm{y}} y)\\ &= a_t + \xi_t\varphi(x,y) + \zeta_t\psi(x,y),\end{aligned} \tag{2}$$

where

$$\begin{aligned}\xi_t &:= b_t\cos\phi_t, \qquad & \varphi(x,y) &:= \cos(2\pi f_{\mathrm{x}} x + 2\pi f_{\mathrm{y}} y),\\ \zeta_t &:= b_t\sin\phi_t, \qquad & \psi(x,y) &:= -\sin(2\pi f_{\mathrm{x}} x + 2\pi f_{\mathrm{y}} y).\end{aligned} \tag{3}$$

In the model Eq.(2), a_t, ξ_t, and ζ_t are parameters. To determine these parameters, this local model is fitted to the observations in the vicinity of the target point by least-squares:

$$(\widehat{a}_t, \widehat{\xi}_t, \widehat{\zeta}_t) := \underset{(a_t,\xi_t,\zeta_t)}{\operatorname{argmin}} \sum_{i\in\mathcal{T}_t} \Big(g_i - \bar{g}_t(x_i, y_i)\Big)^2,$$

where g_i is the pixel value observed at (x_i, y_i). Since the model (2) is linear with respect to a_t, ξ_t, and ζ_t, the least-squares solutions $\widehat{a}_t$, $\widehat{\xi}_t$, and $\widehat{\zeta}_t$ can be analytically obtained as

$$(\widehat{a}_t, \widehat{\xi}_t, \widehat{\zeta}_t)^\top = (\mathbf{A}_t^\top \mathbf{A}_t)^{-1}\mathbf{A}_t^\top \mathbf{g}_t,$$

where, for $\mathcal{T}_t = \{t_1, t_2, \ldots, t_{|\mathcal{T}_t|}\}$ with $|\mathcal{T}_t|$ being the number of elements in the set $\mathcal{T}_t$, the matrix $\mathbf{A}_t$ and the vector $\mathbf{g}_t$ are defined by

$$\mathbf{A}_t := \begin{pmatrix} 1 & \varphi(x_{t_1}, y_{t_1}) & \psi(x_{t_1}, y_{t_1}) \\ 1 & \varphi(x_{t_2}, y_{t_2}) & \psi(x_{t_2}, y_{t_2}) \\ \vdots & \vdots & \vdots \\ 1 & \varphi(x_{|\mathcal{T}_t|}, y_{|\mathcal{T}_t|}) & \psi(x_{|\mathcal{T}_t|}, y_{|\mathcal{T}_t|}) \end{pmatrix}, \quad \mathbf{g}_t := \begin{pmatrix} g_{t_1} \\ g_{t_2} \\ \vdots \\ g_{|\mathcal{T}_t|} \end{pmatrix}.$$

Given $\widehat{\xi}_t$ and $\widehat{\zeta}_t$, an estimate of the surface profile at (x_t, y_t) can be obtained by

$$\widehat{\phi}(x_t, y_t) := \arctan\left(\widehat{\zeta}_t / \widehat{\xi}_t\right) + 2m_t\pi,$$

where m_t is an unknown integer which may be determined by a phase-unwrapping algorithm [13]. In general, the value of 'arctan' can be determined only up to a π range. Nevertheless, since the signs of $\cos\widehat{\phi}(x_t, y_t)$ and $\sin\widehat{\phi}(x_t, y_t)$ can be determined from $\widehat{\xi}_t$ and $\widehat{\zeta}_t$ (see Eq.(3)), $\widehat{\phi}(x_t, y_t)$ can be determined up to a 2π range.

2.2 Behavior of LMF

The measurement principle of the LMF method relies on the assumption that $a(x, y)$, $b(x, y)$, and $\phi(x, y)$ are locally constant around the target point. Although such an assumption may be fulfilled in a flat region of the target object, it is violated, e.g., at the edge of a bump. Setting the vicinity size to a sufficiently small value can mitigate this problem to some extent. However, this in turn degrades the noise reduction power because the number of samples used for estimation is reduced.

In order to illustrate this trade-off phenomenon, we performed a computer simulation. The simulated target object is illustrated in Figure 1(a). We generated a fringe image by Eq.(1) with $a(x, y) = b(x, y) = 1$, and added Gaussian noise with mean 0 and standard deviation 0.1. Figures 1(b) and (c) depict the fringe image. Figures 1(d)–(i) depict surface profiles estimated by the LMF method with vicinity size 3×3 (small), 5×5 (medium), and 7×7 (large), respectively; below the figures, the *root mean square error* (RMSE) between the true surface profile ϕ and its estimate $\widehat{\phi}$ is described:

$$\mathrm{RMSE}_\phi := \sqrt{\frac{1}{|\mathcal{T}|}\sum_{t\in\mathcal{T}}\left(\widehat{\phi}(x_t, y_t) - \phi(x_t, y_t)\right)^2}, \tag{4}$$

where $\mathcal{T}$ is the set of pixel indices for the entire image.

When the vicinity size is large (see Figures 1(f) and (i)), the number of samples to be used for estimating the surface profile is large and thus the influence of noise can be sufficiently suppressed. As a result, the estimated surface profile tends to be smooth. However, the locally flat assumption is heavily violated around the sharp edges, and consequently the sharp edges become blunt.

On the other hand, when the vicinity size is small (see Figures 1(d) and (g)), the number of samples to be used for estimating the surface profile is small and thus the estimated surface profile is highly noisy. However, since the locally flat assumption is well fulfilled, the sharp edges are clearly recovered.

If the vicinity size is determined so that the trade-off between noise reduction and local flatness is well controlled, the obtained surface profile preserves both sharp edges and smooth surface, resulting in the smallest RMSE (see Figures 1(e) and (h)).

The above simulation result shows that, given that the vicinity size is chosen optimally, the LMF method gives accurate estimation. Since this was a computer simulation where

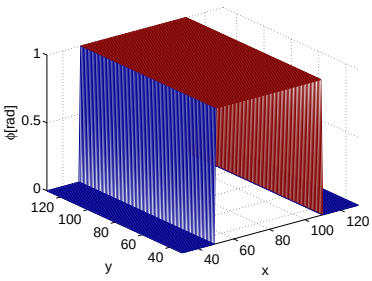

(a) Target object

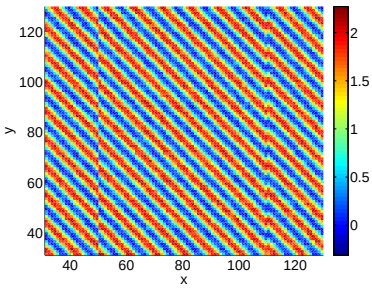

(b) Fringe image

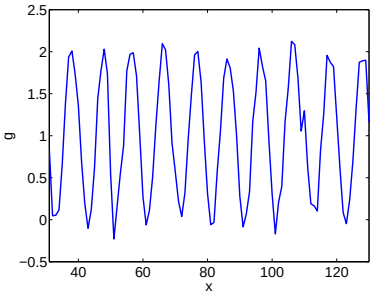

(c) Fringe image ($y = 80$)

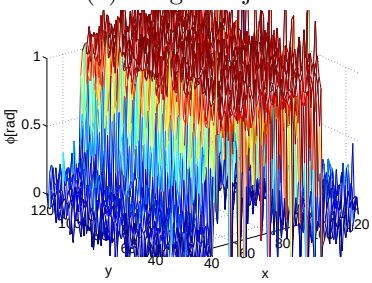

(d) LMF (3×3), $\mathrm{RMSE}_\phi = 0.1377$[rad]

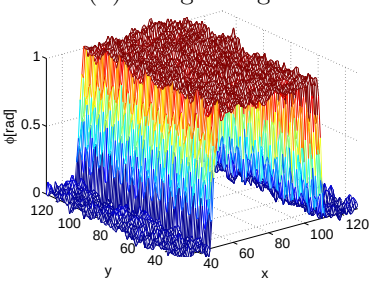

(e) LMF (5×5), $\mathrm{RMSE}_\phi = 0.1001$[rad]

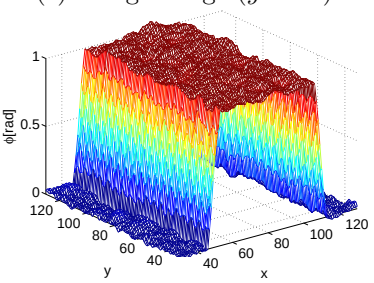

(f) LMF (7×7), $\mathrm{RMSE}_\phi = 0.1083$[rad]

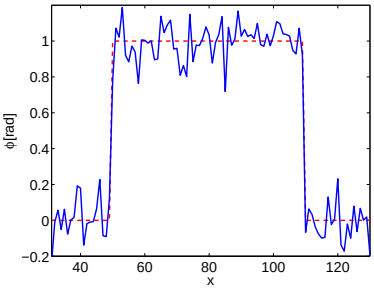

(g) LMF (3×3, $y = 80$)

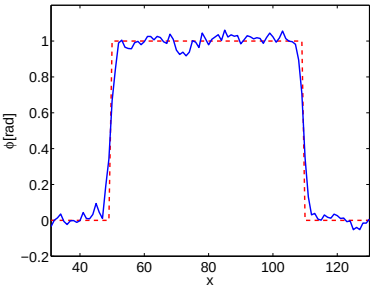

(h) LMF (5×5, $y = 80$)

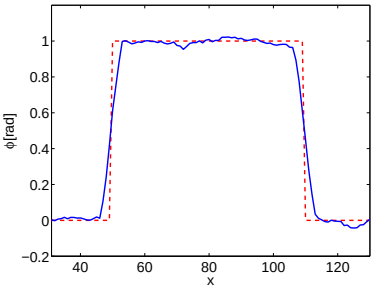

(i) LMF (7×7, $y = 80$)

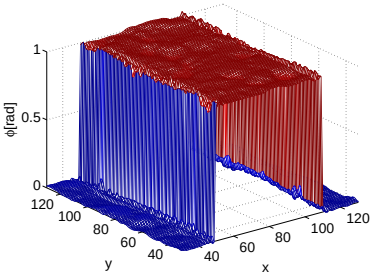

(j) IRLMF with automatic parameter optimization ($d_1 = 6$, $d_2 = 30$, $c = 10^{-4}$) $\mathrm{RMSE}_\phi = 0.0149$[rad]

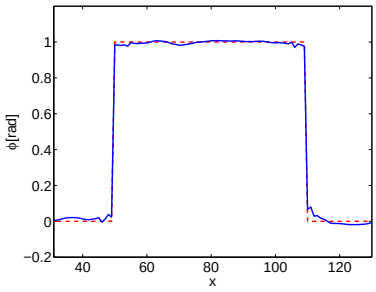

(k) IRLMF with automatic parameter optimization ($y = 80$)

Figure 1: Experimental results for the artificial sharp bump.

the true surface profile is known, the vicinity size could be manually optimized. However, in practice, such a manual parameter choice is not possible without strong prior knowledge on the true surface profile. This is a critical limitation of the LMF method for practical use.

The goal of this paper is to overcome this limitation by providing a method for automatically determining the vicinity size, which is described below.

2.3 Automatic Parameter Optimization for LMF

Ideally, we would like to determine the vicinity size so that RMSE_ϕ defined by Eq.(4) is minimized. However, since the true surface profile is not accessible in reality, RMSE_ϕ cannot be directly evaluated. To cope with this problem, we instead propose to use RMSE between the observed fringe image $\{g_t\}_{t\in\mathcal{T}}$ and its estimate $\{\widehat{g}_t\}_{t\in\mathcal{T}}$:

$$\mathrm{RMSE}_\mathrm{g} := \sqrt{\frac{1}{|\mathcal{T}|}\sum_{t\in\mathcal{T}}(\widehat{g}_t - g_t)^2}.$$

The fact that the observed fringe image $\{g_t\}_{t\in\mathcal{T}}$ is estimated accurately implies that the model parameters are determined appropriately. Consequently, the true surface profile $\{\phi(x_t, y_t)\}_{t\in\mathcal{T}}$ would be accurately estimated.

However, naively obtaining an estimate $\widehat{g}_t$ based on the local model Eq.(2) with the least-squares solutions $\widehat{a}_t$, $\widehat{\xi}_t$, and $\widehat{\zeta}_t$ by

$$\widehat{a}_t + \widehat{\xi}_t\varphi(x_t, y_t) + \widehat{\zeta}_t\psi(x_t, y_t)$$

significantly under-estimates the error since the observed sample g_t itself is used for obtaining $\widehat{g}_t$. To avoid this under-estimation, we exclude the observed data g_t from the data set when estimating $\widehat{g}_t$. Thus, when estimating the surface profile at (x_t, y_t), we solve the following least-squares problem:

$$(\widetilde{a}_t, \widetilde{\xi}_t, \widetilde{\zeta}_t) := \operatorname*{argmin}_{(a_t,\xi_t,\zeta_t)} \sum_{i\in\mathcal{T}_t\backslash t} \Big(g_i - \bar{g}_t(x_i, y_i)\Big)^2,$$

where $\mathcal{T}_t\backslash t$ denotes the set $\mathcal{T}_t$ without element t. The solutions $\widetilde{a}_t$, $\widetilde{\xi}_t$, and $\widetilde{\zeta}_t$ can still be computed analytically, in the same way as $\widehat{a}_t$, $\widehat{\xi}_t$, and $\widehat{\zeta}_t$, and an estimate $\widehat{g}_t$ can be obtained using the local model Eq.(2) with $\widetilde{a}_t$, ξ_t, and ζ_t as

$$\widehat{g}_t := \widetilde{a}_t + \widetilde{\xi}_t\varphi(x_t, y_t) + \widetilde{\zeta}_t\psi(x_t, y_t).$$

Based on RMSE_g with the above estimate $\{\widehat{g}_t\}_{t\in\mathcal{T}}$, we determine the vicinity size so that RMSE_g is minimized.

We computed the values of RMSE_g for the artificial data used in Section 2.2. Figure 2(a) depicts the values of RMSE_g for vicinity size $s\times s$ with $s = 3, 5, \ldots, 11$. RMSE_g is minimized when $s = 5$, which is chosen as the best vicinity size. Figure 2(b) depicts the values of RMSE_ϕ for $s = 3, 5, \ldots, 11$, which is also minimized at $s = 5$. Thus, for this artificial data, the truly best vicinity size (i.e., 5×5) can be chosen by the proposed method.

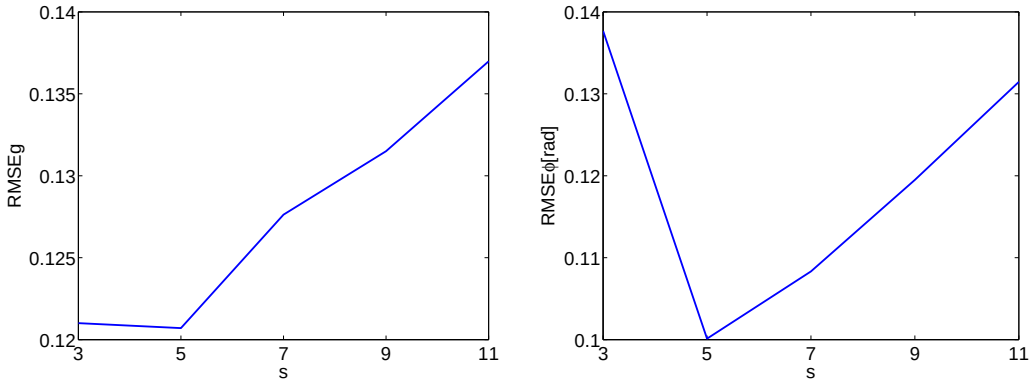

(a) $\mathrm{RMSE_g}$ of each s (b) RMSE_ϕ of each s

Figure 2: $\mathrm{RMSE_g}$ and RMSE_ϕ as functions of vicinity size s for the artificial sharp bump.

3 Automatic Parameter Determination for Iteratively-Reweighted Local Model Fitting

As shown in the previous section, the tuning parameter (i.e., the vicinity size) of the LMF method can be successfully determined by the proposed method. On the other hand, one of the limitations of the above approach is that the vicinity size is controlled *globally*. If the vicinity size was controlled *locally* in a more adaptive manner (e.g., using a smaller vicinity size around edges and using a larger vicinity size in a flat region), the measurement accuracy would be further improved. Based on this idea, the *iteratively-reweighted LMF* (IRLMF) method [12] was developed recently. In this section, we first review the IRLMF method in a slightly generalized manner, and then we extend our automatic parameter optimization technique to the IRLMF method.

3.1 The Iteratively-Reweighted Local Model Fitting Method

The IRLMF algorithm consists of the *weighted LMF* (WLMF) method, which involves the following weighted least-squares problem:

$$(\widehat{a}_t, \widehat{\xi}_t, \widehat{\zeta}_t) := \underset{(a_t,\xi_t,\zeta_t)}{\operatorname{argmin}} \left[\sum_{i \in \mathcal{T}_t} w_{t,i} (g_i - \bar{g}_t(x_i, y_i))^2 \right],$$

where $w_{t,i}$ ($\in [0,1]$) is the weight for point (x_i, y_i) in the vicinity of the target point (x_t, y_t). The above weighted least-squares solutions $\widehat{a}_t$, $\widehat{\xi}_t$, and $\widehat{\zeta}_t$ can be obtained analytically as

$$(\widehat{a}_t, \widehat{\xi}_t, \widehat{\zeta}_t)^\top = (\mathbf{A}_t^\top \mathbf{W}_t \mathbf{A}_t)^{-1} \mathbf{A}_t^\top \mathbf{W}_t \mathbf{g}_t,$$

where $\mathbf{W}_t$ is the diagonal matrix with diagonal elements $w_{t,t_1}, w_{t,t_2}, \ldots, w_{t,|\mathcal{T}_t|}$. If the weights take either zero or one, choosing the weights corresponds to determining the shape and size of the vicinity region. Here, the weights are allowed to take real values in $[0,1]$, meaning that

the vicinity regions are determined in a 'soft' manner. Furthermore, the weights can depend on the target point (x_t, y_t), allowing the vicinity regions to be chosen in a local manner. Thus, WLMF is more flexible than the original LMF method.

Typically, the weight $w_{t,i}$ are required to take a large value if (x_i, y_i) is close to (x_t, y_t) in the (x, y)-space and if $\phi(x_i, y_i)$ is close to $\phi(x_t, y_t)$ in the ϕ-space. For example, the following weight satisfies this requirement:

$$\sqrt{1 - d^{-2}\left((x_i - x_t)^2 + (y_i - y_t)^2\right)} \cdot \left(1 + c^{-1}(\phi(x_i, y_i) - \phi(x_t, y_t))^2\right)^{-1},$$

where d and c are tuning parameters. However, since the true surface profile ϕ is unknown, the paper [12] proposed the following two-step procedure: First, initial surface estimation is performed for designing the weight pattern; in our implementation, the WLMF method with the following weight pattern is used:

$$w_{t,i}^{(1)} := \sqrt{1 - d_1^{-2}\left((x_i - x_t)^2 + (y_i - y_t)^2\right)}. \tag{5}$$

Then the final estimation is performed by the WLMF method; in our implementation, the following weight pattern is used:

$$w_{t,i}^{(2)} := \sqrt{1 - d_2^{-2}\left((x_i - x_t)^2 + (y_i - y_t)^2\right)} \cdot \left(1 + c^{-1}(\widetilde{\phi}(x_i, y_i) - \widetilde{\phi}(x_t, y_t))^2\right)^{-1}, \tag{6}$$

where $\widetilde{\phi}$ is the surface profile obtained by the above initial estimation. This method is called the IRLMF method.

The paper [12] demonstrated that IRLMF works excellently, given that the tuning parameters are determined appropriately. However, IRLMF involves three tuning parameters (d_1, d_2, and c), and manually choosing them appropriately is highly cumbersome in practice. Below, we extend our automatic parameter selection method described in the previous section to IRLMF, and show its practical usefulness through numerical experiments.

3.2 Automatic Parameter Optimization for IRLMF

Here we describe our automatic parameter optimization algorithm for IRLMF, and report the results of computer simulation and actual experiments.

3.2.1 Algorithm

Our proposed procedure is described as follows:

1. Initial estimation is performed in a hold-out manner by WLMF with weight pattern defined by Eq.(5) for various candidate parameter values d_1.

2. For each d_1, the second estimation is performed in a hold-out manner by WLMF with weight pattern defined by Eq.(6) for various candidate parameter values d_2 and c.

3. $\mathrm{RMSE}_{\mathrm{g}}$ is computed in a hold-out manner for all combination of d_1, d_2, and c.

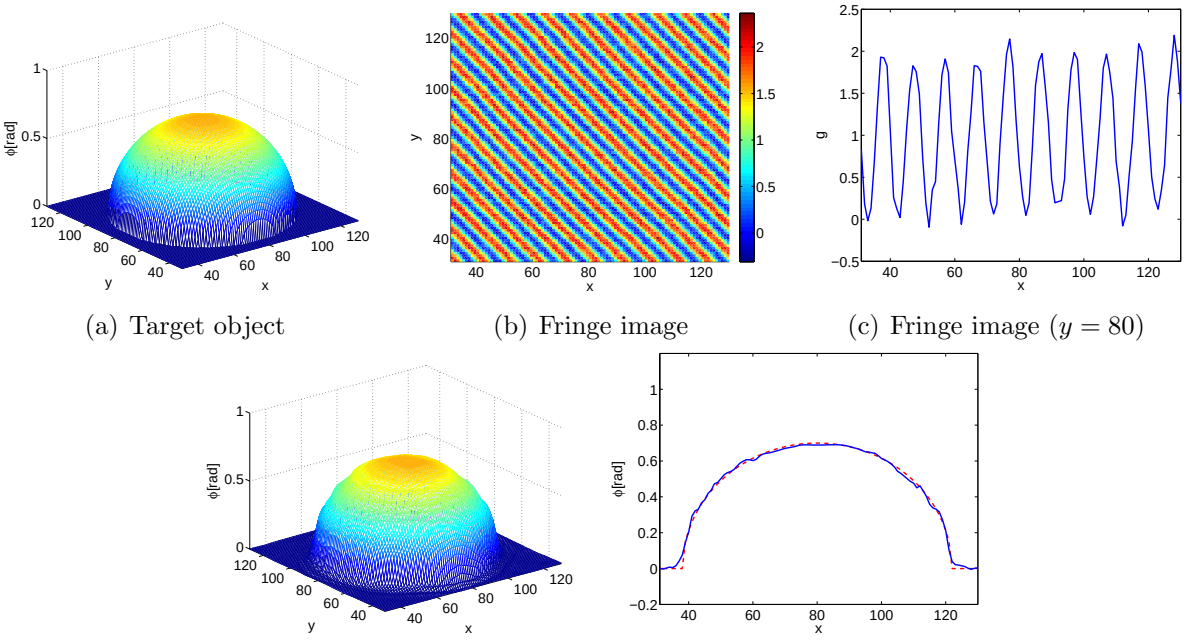

(a) Target object (b) Fringe image (c) Fringe image ($y = 80$)

(d) IRLMF with automatic parameter optimization ($d_1 = 12$, $d_2 = 30$, $c = 10^{-4}$) $\mathrm{RMSE}_\phi = 0.0143$[rad]

(e) IRLMF with automatic parameter optimization ($y = 80$)

Figure 3: Experimental results for the artificial sphere bump.

4. The parameter values $(\widehat{d}_1, \widehat{d}_2, \widehat{c})$ that minimize the hold-out RMSE_g are chosen.

5. Initial estimation is performed using all the samples (i.e., no hold-out) by WLMF with weight pattern defined by Eq.(5) for $\widehat{d}_1$.

6. Final estimation is performed using all the samples (i.e., no hold-out) by WLMF with weight pattern defined by Eq.(6) for $\widehat{d}_2$ and $\widehat{c}$.

3.2.2 Computer Simulation

We applied the above automatic parameter selection procedure to the artificial data used in Section 2.2. The tuning parameter values are chosen from $d_1 \in \{3, 6, 9, 12, 15\}$, $d_2 \in \{10, 15, 20, 25, 30\}$, and $c \in \{10^{-5}, 10^{-4}, 10^{-3}, 10^{-2}, 10^{-1}\}$, respectively. Figures 1(j)(k) depict the simulation results obtained by IRLMF combined with our automatic parameter selection procedure, showing that both sharp edges and smooth surface are preserved much better than the optimized LMF method (see Figures 1(e)(h)). Consequently, RMSE_ϕ becomes much smaller than that of the LMF method.

We performed similar computer simulations also for other artificial data: a sphere bump (Figure 3) and a fish-shaped object (Figure 4), showing that IRLMF equipped with our automatic parameter selection procedure still works excellently.

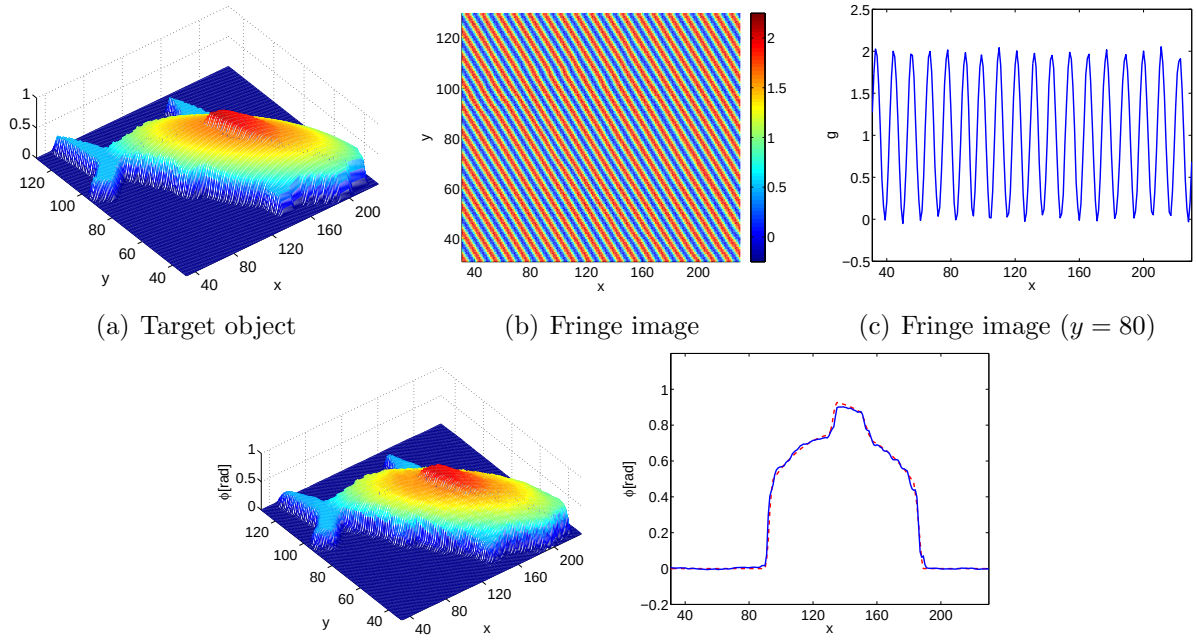

(a) Target object (b) Fringe image (c) Fringe image ($y = 80$)

(d) IRLMF with automatic parameter optimization ($d_1 = 3$, $d_2 = 10$, $c = 10^{-3}$) $\mathrm{RMSE}_\phi = 0.0167$[rad]

(e) IRLMF with automatic parameter optimization ($y = 80$)

Figure 4: Experimental results for the artificial fish-shaped object.

3.2.3 Actual Experiments

Finally, we report the results of actual experiments. We obtained interference images by using the optical surface profiler *SP-500* developed by Toray Engineering Co., Ltd. [14], which allows a full-field measurement of 512×480 pixels (the actual size is 0.80 [mm] $\times$ 0.72 [mm]). In our experiments, we focused on the 120×120 pixels in the middle of the image. Each pixel takes an integer value between 0 and 255 (i.e., 8-bit intensity), and the wavelength of the light source is 603 [nm] (we used a narrow-band optical filter).

Figure 5(a) illustrates the surface profile of the target object, and Figures 5(b)(c) depict the observed fringe image. The surface profile obtained by the proposed method is depicted in Figures 5(d)(e), showing that the sharp edges and smooth surface are accurately recovered.

4 Conclusions

Single-shot methods are faster and more robust against disturbance such as vibration than multiple-shot methods, and the LMF method has various practical advantages over other single-shot methods. However, the LMF method requires the locally flat assumption, and its accuracy can be degraded by the violation of this assumption. Appropriately choosing the size of the local region is the key to mitigating this problem, but this is often cumbersome

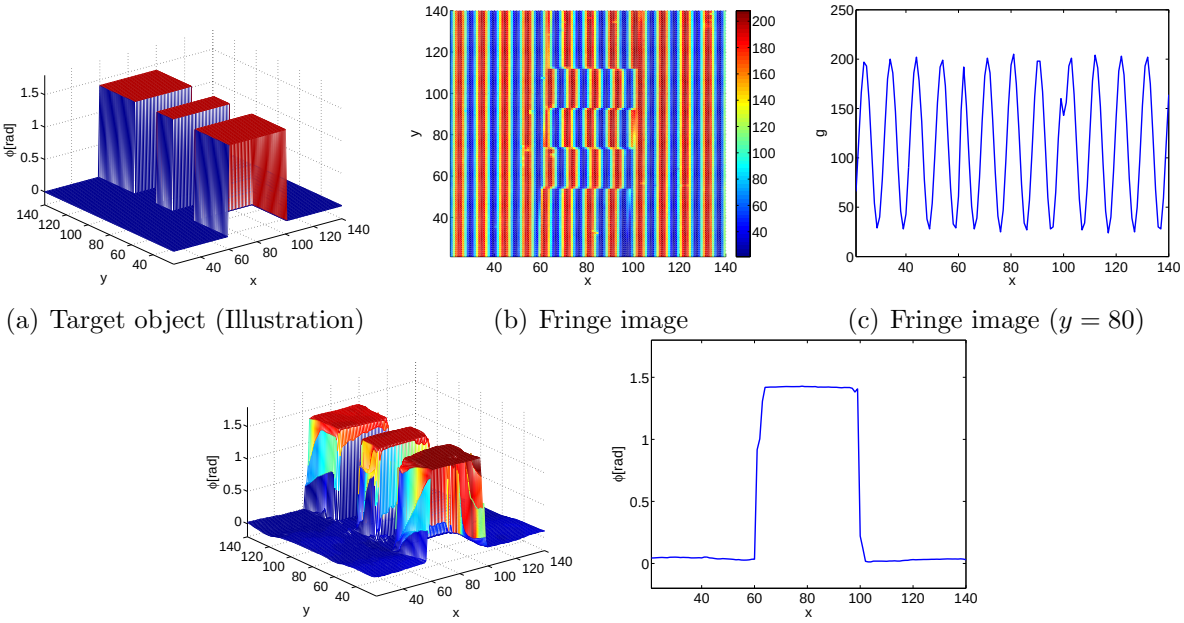

(a) Target object (Illustration) (b) Fringe image (c) Fringe image ($y = 80$)

(d) IRLMF with automatic parameter optimization ($d_1 = 3$, $d_2 = 10$, $c = 10^{-3}$)

(e) IRLMF with automatic parameter optimization ($y = 80$)

Figure 5: Actual measurement results.

in practice. In this paper, we proposed an automatic parameter optimization procedure for LMF, which is based on the hold-out estimation of the fringe image. We further extended the proposed method to a more flexible variant of LMF called IRLMF, and demonstrated the usefulness of the proposed approach through simulation and actual experiments.

Due to exhaustive parameter search, the computation time of the proposed method is proportional to the number of parameter combinations. However, we note that the parameter search can easily be carried out in parallel, for example, using grid computers or graphics processing units. Furthermore, such parameter tuning is necessary only *once* in advance to create a "recipe" for the target experiment. Thus, the high computational cost of the proposed method would not be critical in practice. Nevertheless, improving the computational efficiency would be an important future work.

References

[1] J. H. Brunning, D. R. Herriott, J. E. Gallagher, D. P. Rosenfeld, A. D. White, and D. J. Brangaccio, "Digital Wave Front Measuring Interferometer for Testing Optical Surface and Lenses," Applied Optics **13**(11), 2693–2703 (1974).

[2] M. Takeda, H. Ina, and S. Kobayashi, "Fourier-Transform Method of Fringe-Pattern Analysis for Computer-Based Topography and Interferometry," Journal of Optical Society of America **72**(1), 156–160 (1982).

[3] J. Kato, I. Yamaguchi, T. Nakamura, and S. Kuwashima, "Video-Rate Fringe Analyzer Based on Phase-Shifting Electronic Moiré Patterns," Applied Optics **36**(32), 8403–8412 (1997).

[4] Q. Kemao, "Windowed Fourier Transform for Fringe Pattern Analysis," Applied Optics **43**(13), 2695–2702 (2004).

[5] D. C. Williams, N. S. Nassar, J. E. Banyard, and M. S. Virdee, "Digital Phase-Step Interferometry: A Simplified Approach," Optics & Laser Technology **23**(3), 147–150 (1991).

[6] N. Brock, J. Hayes, B. Kimbrough, J. Millerd, M. North-Morris, M. Novak, and J. C. Wyant, "Dynamic Interferometry," in *Novel Optical Systems Design and Optimization VIII, Proceedings of SPIE*, J. M. Sasián, R. J. Koshel, and R. C. Juergens, eds., vol. 5875, pp. 1–10 (2005).

[7] M. Sugiyama, H. Ogawa, K. Kitagawa, and K. Suzuki, "Single-Shot Surface Profiling by Local Model Fitting," Applied Optics **45**(31), 7999–8005 (2006).

[8] W. H. Su, "Color-Encoded Fringe Projection for 3D Shape Measurements," Optics Express **15**(20), 13,167–13,181 (2007).

[9] H. J. Chen, J. Zhang, D. J. Lv, and J. Fang, "3-D Shape Measurement by Composite Pattern Projection and Hybrid Processing," Optics Express **15**(19), 12,318–12,330 (2007).

[10] W. H. Su, "Projected Fringe Profilometry Using the Area-Encoded Algorithm for Spatially Isolated and Dynamic Objects," Optics Express **16**(4), 2590–2596 (2008).

[11] Z. Zhang, D. P. Towers, and C. E. Towers, "Snapshot Color Fringe Projection for Absolute Three-Dimensional Metrology of Video Sequences," Applied Optics **49**(31), 5947–5953 (2010).

[12] N. Kurihara, M. Sugiyama, H. Ogawa, K. Kitagawa, and K. Suzuki, "Iteratively-Reweighted Local Model Fitting Method for Adaptive and Accurate Single-Shot Surface Profiling," Applied Optics **49**(22), 4270–4277 (2010).

[13] M. Takeda and T. Abe, "Phase Unwrapping by a Maximum Cross-Amplitude Spanning Tree Algorithm: A Comparative Study," Optical Engineering **35**(8), 2345–2351 (1996).

[14] Toray Engineering Co., Ltd., "SP-500," `http://www.toray-eng.com/lcd/inspection/lineup/sp-500.html`.